8912 *Biochemistry* **2010,** *49,* 8912–8921
DOI: 10.1021/bi100781f

BIOCHEMISTRY
including biophysical chemistry & molecular biology
Article

Reaction Cycle of the Dissimilatory Sulfite Reductase from *Archaeoglobus fulgidus*[†,‡]

Kristian Parey,[§,∥] Eberhard Warkentin,[§] Peter M. H. Kroneck,*[,⊥] and Ulrich Ermler*[,§]

[§]*Max-Planck-Institut für Biophysik, Max-von-Laue-Strasse 3, D-60438 Frankfurt, Germany,* [∥]*Max-Planck-Institut für Terrestrische Mikrobiologie, Karl-von-Frisch-Strasse, D-35043 Marburg, Germany, and* [⊥]*Fachbereich Biologie, Mathematisch-Naturwissenschaftliche Sektion, Universität Konstanz, Universitätsstrasse 10, D-78457 Konstanz, Germany*

Received May 18, 2010; Revised Manuscript Received August 5, 2010

ABSTRACT: A vital process in the biogeochemical sulfur cycle is the dissimilatory sulfate reduction pathway in which sulfate (SO_4^{2-}) is converted to hydrogen sulfide (H_2S). Dissimilatory sulfite reductase (dSir), its key enzyme, hosts a unique siroheme-[4Fe-4S] cofactor and catalyzes the six-electron reduction of sulfite (SO_3^{2-}) to H_2S. To explore this reaction, we determined the X-ray structures of dSir from the archaeon *Archaeoglobus fulgidus* in complex with sulfite, sulfide (S^{2-}), carbon monoxide (CO), cyanide (CN^-), nitrite (NO_2^-), nitrate (NO_3^-), and phosphate (PO_4^{3-}). Activity measurements indicated that dSir of *A. fulgidus* reduces, besides sulfite and nitrite, thiosulfate ($S_2O_3^{2-}$) and trithionate ($S_3O_6^{2-}$) and produces the latter two compounds besides sulfide. On this basis, a three-step mechanism was proposed, each step consisting of a two-electron transfer, a two-proton uptake, and a dehydration event. In comparison, the related active site structures of the assimilatory sulfite reductase (aSir)− and dSir−SO_3^{2-} complexes reveal different conformations of Argα170 and Lysα211 both interacting with the sulfite oxygens (its sulfur atom coordinates the siroheme iron), a sulfite rotation of ∼60° relative to each other, and different access of solvent molecules to the sulfite oxygens from the active site cleft. Therefore, solely in dSir a further sulfite molecule can be placed in van der Waals contact with the siroheme-ligated sulfite or sulfur−oxygen intermediates necessary for forming thiosulfate and trithionate. Although reported for dSir from several sulfate-reducing bacteria, the in vivo relevance of their formation is questionable.

Since the early stages of Earth's biogeochemical evolution (*1*), sulfur compounds have been recruited by microbes as electron donors or acceptors for energy conservation (*2*, *3*) and for the biosynthesis of sulfur-containing amino acids and cofactors (*4*). Both processes, termed dissimilatory and assimilatory, use the element in oxidation states from S^{+VI} to S^{-II}, with sulfate (SO_4^{2-}), elemental sulfur ($\langle S^0 \rangle$), and hydrogen sulfide (H_2S) being the most abundant sulfur compounds on Earth. The dissimilatory reduction of sulfate to hydrogen sulfide proceeds via three major steps catalyzed by ATP sulfurylase (ATP + SO_4^{2-} → adenosine 5′-phosphosulfate + PP_i), adenosine-5′-phosphosulfate reductase (adenosine 5′-phosphosulfate → AMP + SO_3^{2-}), and sulfite reductase (SO_3^{2-} → H_2S). The oxidative process runs in the reverse direction. The assimilatory sulfite reduction includes an additional phosphorylation step at the adenosine 5′-phosphosulfate level.

Sulfite reductases are key enzymes of sulfur metabolism (*5*, *6*) because they catalyze the $SO_3^{2-} + 6e^- + 8H^+ \rightarrow H_2S + 3H_2O$ complex six-electron reduction. They have been subdivided correspondingly into dissimilatory and assimilatory enzyme types (dSir[1] and aSir, respectively) (*5*, *7*). Two aberrant low-molecular weight sulfite reductases, an assimilatory type (*8*) and a dissimilatory type (*9*), have been described recently. These enzymes are not well understood and therefore not subjects of this report. In addition, the sulfite reductase family includes assimilatory nitrite reductases (*10*) that catalyze the six-electron reduction of nitrite to ammonia ($NO_2^- + 6e^- + 7H^+ \rightarrow NH_3 + 2H_2O$).

dSirs and aSirs reveal both common and distinct properties. Both classes contain a siroheme-Fe/S center that is composed of a reduced porphyrin ring of the isobacteriochlorin class bridged to a [4Fe-4S] cluster via a cysteine thiolate (*11*). This magnetically coupled metallo-cofactor possesses interesting spectroscopic properties. Thus, the EPR spectra of dSir and aSir in the oxidized state exhibited signals assigned to an $S = {}^5/_2$ spin state (*12*) resulting from a coupling between the siroheme and the [4Fe-4S] cluster. dSir additionally exhibited resonance signals from an $S = {}^9/_2$ system (*13*) whose molecular basis is not understood. X-ray structural analysis of aSirs from *Escherichia coli* (*14*) and *Mycobacterium tuberculosis* (*15*), assimilatory spinach nitrite reductase (*16*), and dSirs from *Archaeoglobus fulgidus* (*17*) and *Desulfovibrio vulgaris* (*18*) reveals an architecturally related trilobal core structure harboring the unique siroheme-[4Fe-4S] site in the center of three α/β domains. The core of dSir is organized as an αβ heterodimer that forms a heterotetrameric $(\alpha\beta)_2$ complex (Figure 1A). In several sulfate-reducing mircoorganisms, the αβ units of dSir associate with one or two smaller subunits, γ and δ (*19*, *20*). Whereas subunit δ is assigned a regulatory role (*21*), subunit γ is postulated to be directly involved in sulfite reduction (*18*, *22*, *23*). In the impressive structure of the dSir $\alpha_2\beta_2\gamma_2$ complex of *D. vulgaris*, the C-terminal arm of subunit γ extends toward the siroheme-[4Fe-4S]

[†]This work was supported by the Max Planck Society. K.P. is grateful to Rudolf K. Thauer (MPI for Terrestrial Microbiology, Marburg) for financial support.

[‡]We dedicate this work to F. Ann Walker on the occasion of her 70th birthday.

*To whom correspondence should be addressed. U.E.: telephone, +49-(0)69-6303-1054; fax, +49-(0)69-6303-1002; e-mail, ulrich.ermler@biophys.mpg.de. P.M.H.K.: telephone, +49-(0)7531-88-2103; fax, +49-(0)7531-88-2966; e-mail, peter.kroneck@uni-konstanz.de.

[1]Abbreviations: dSir, dissimilatory sulfite reductase; aSir, assimilatory sulfite reductase; rmsd, root-mean-square deviation.

 Published on Web 09/07/2010

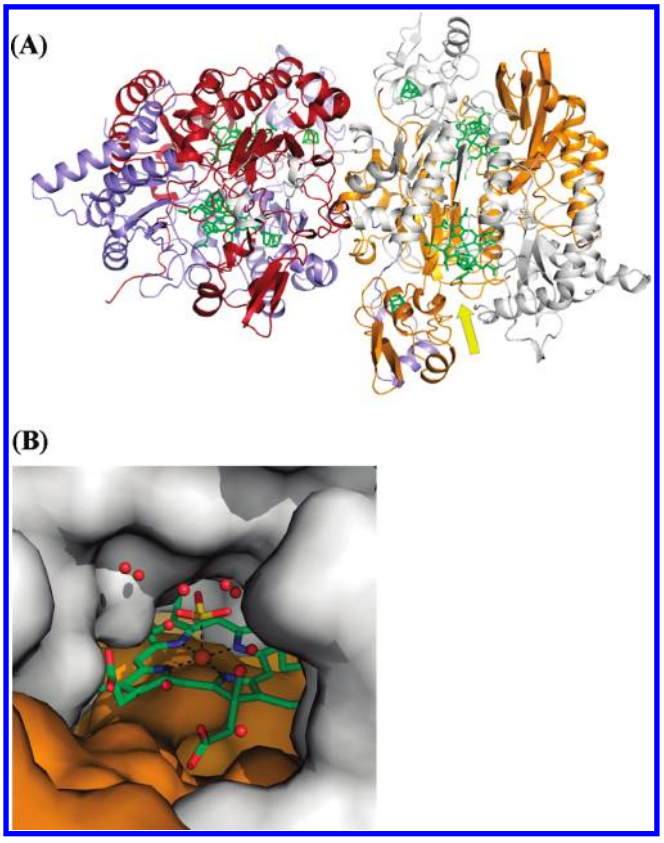

FIGURE 1: Overall architecture of dSir from *A. fulgidus* using the highly resolved structure of the dSir−SO_3^{2-} complex. (A) Ribbon diagram of the $\alpha_2\beta_2$ heterotetramer with the α subunits colored red and orange, the β subunits light blue and gray, and the cofactors green. The active site funnel is indicated by a yellow arrow. (B) Molecular surface representation focusing on the active site funnel. The sulfite ion (yellow for S and red for O) ligated to the catalytic siroheme iron (green for C, blue for N, and brown and Fe) is connected to the bulk solvent via a chain of firmly bound solvent molecules (red spheres).

cofactor and a strictly conserved cysteine could thus transfer two electrons to an intermediate sulfur−oxygen species bound to the siroheme iron (*18*). In contrast, the core of aSir is a monomeric protein built of two fused modules that are structurally related to subunits α and β (*5*) except for a ferredoxin domain only inserted into the subunits of dSir. The [4Fe-4S] cluster of this ferredoxin domain is considered as the terminal electron carrier to the siroheme-[4Fe-4S] center in dSir (*17*, *18*). The monomeric aSir core acts (depending on the organism) in combination with an electron-delivering ferredoxin or is integrated into an $\alpha_4\beta_8$ multisubunit complex in which the FAD-containing β subunit funnels the electrons to the core (*24*, *25*). While each aSir monomer binds one siroheme-[4Fe-4S] center, dSir harbors two of them within each $\alpha\beta$ heterodimer (Figure 1A) (*17*, *18*). Surprisingly, only one siroheme-[4Fe-4S] center in each $\alpha\beta$ heterodimer is catalytically active, whereas the access to the second center is blocked. In the crystal structure of the *D. vulgaris* dSir (*18*), the corresponding inactive site is occupied by sirohydrochlorin, the demetalated form of siroheme. Both analogies and differences in aSir and dSir have allowed a scenario for the evolution of sulfite reductases to be postulated (*17*).

The reactions of aSir and dSir reveal substantial differences. While aSir usually converts sulfite directly to hydrogen sulfide without the release of intermediates, dSir of various bacteria produce, or to react with, other sulfur compounds such as

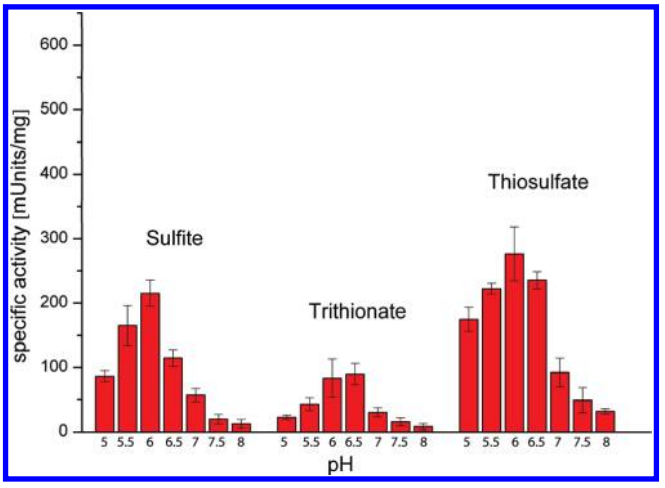

FIGURE 2: Specific activities of *A. fulgidus* dSir for the reduction of sulfite, thiosulfate, and trithionate at different pH values. The following buffers were used: 50 mM sodium citrate (pH 5.0−5.5) and 50 mM KP_i (pH 6.0−8.0). The specific activities were measured at a substrate concentration of 3 mM, which is close to the saturation concentrations of all three substrates.

thiosulfate ($S_2O_3^{2-}$) or trithionate ($S_3O_6^{2-}$) (*26*). In this work, we will report on the reactivity of dSir of *A. fulgidus* (*27*) with respect to sulfite and related sulfur oxyanions, and with respect to nitrite. The catalytic siroheme-[4Fe-4S] center of dSir was probed and a mechanism proposed for the six-electron reduction of sulfite on the basis of the crystal structures of dSir in complex with the substrate sulfite and the product sulfide, with the classical heme ligands cyanide and carbon monoxide, and with the oxyanions thiosulfate, trithionate, nitrite, nitrate, and phosphate.

MATERIALS AND METHODS

Analytical Methods. dSir of *A. fulgidus* was purified under exclusion of dioxygen as described previously (*17*) and stored in 50 mM KP_i (pH 7.0) and 150 mM NaCl. Its concentration was determined with bicinchoninic acid (*28*). The enzymatic activity for the reduction of sulfite, trithionate, and thiosulfate was colorimetrically determined at 83 °C using photochemically reduced methyl viologen as the electron donor (Figure 2). Prior to activity measurements, thiosulfate and trithionate were analyzed by HPLC to ensure that they did not contain sulfite. The activity assay consisted of 40 mM sodium oxalate, 0.75 mM methyl viologen, 10 μM 5-deazaflavin, 50 mM sodium citrate (pH 5.0−5.5), or 50 mM KP_i (pH 6.0−8.0). Enzyme (final concentration of 53 pM) and substrate (final concentration of 3 mM) were added to a cuvette sealed with a rubber septum using a gastight syringe. The reaction was monitored by following the decrease in absorbance at 732 nm (ε_{732} = 3150 M^{-1} cm^{-1}) as a result of methyl viologen oxidation (*29*). Nitrite reductase activity was determined following the formation of ammonia (*30*). All assays were conducted in triplicate, with standard deviations shown as error bars (Figure 2). Formation and turnover of trithionate and thiosulfate were followed by the cyanolysis method and subsequent photometric determination of the Fe(III)−thiocyanate complex at 460 nm (*31*, *32*); formation of sulfide was followed at 670 nm with the methylene blue method (*33*, *34*). In parallel, the formation of hydrogen sulfide was monitored on a filter paper soaked either with 20 μL of lead(II) acetate or with 20 μL of cadmium(II) acetate (10%, by mass) and 20 μL of NaOH (12%, by mass) (*35*).

Table 1: Data Collection and Refinement Statistics

	dSir−SO_3^{2-}	dSir−CN^-	dSir−CO	dSir−NO_3^-	dSir−NO_2^-	dSir−PO_4^{3-}	dSir−S^{2-}
Data Collection							
soaking conditions (final concentrations)	50 mM Na_2SO_3	10 mM Cr(II) EDTA with 10 mM KCN	1 bar CO	50 mM $NaNO_3$	50 mM $NaNO_2$	50 mM KP_i	10 mM Cr(II) EDTA with 10 mM Na_2S
wavelength (Å)	0.9999	1.0	1.0001	0.9998	1.0	0.9998	1.0
resolution range (Å) (last shell)	50.0−1.80 (1.80−1.91)	50.0−1.90 (1.90−2.00)	50.0−1.90 (1.90−2.00)	50.0−2.30 (2.30−2.44)	50.0−2.01 (2.01−2.13)	50.0−2.31 (2.31−2.45)	50.0−2.33 (2.33−2.45)
no. of unique reflections (last shell)	166132 (86856)	134065 (66700)	140631 (66677)	151092 (44806)	102627 (9280)	75665 (11623)	64472 (5659)
multiplicity	3.6	3.4	3.2	1.9	3.4	3.2	2.6
unit cell dimensions	a = 94.8 Å b = 68.7 Å c = 147.5 Å β = 107.5°	a = 94.5 Å b = 68.7 Å c = 145.6 Å β = 107.6°	a = 94.8 Å b = 69.3 Å c = 146.3 Å β = 107.7°	a = 94.9 Å b = 69.2 Å c = 146.7 Å β = 107.5°	a = 95.0 Å b = 69.1 Å c = 145.6 Å β = 107.5°	a = 94.7 Å b = 68.3 Å c = 146.7 Å β = 107.5°	a = 94.9 Å b = 68.5 Å c = 141.9 Å β = 107.5°
completeness (%)	98.5 (94.4)	95.4 (95.9)	98.5 (99.8)	96.3 (94.0)	84.8 (47.8)	96.2 (92.2)	86.6 (54.6)
R_{sym} (%)	13.1 (58.3)	7.8 (53.5)	13.8 (74.0)	15.3 (44.0)	7.4 (37.6)	8.7 (53.3)	10.2 (28.6)
$I/\sigma(I)$	7.0 (2.5)	11.4 (3.2)	8.4 (2.3)	4.2 (2.1)	12.0 (2.9)	10.7 (2.5)	9.0 (3.3)
Refinement Statistics							
no. of residues, sirohemes, [4Fe-4S] clusters, and solvent molecules	1566, 4, 8, 1103	1566, 4, 8, 248	1566, 4, 8, 557	1566, 4, 8, 139	1566, 4, 8, 482	1566, 4, 8, 182	1566, 4, 8, 114
resolution range (Å) (last shell)	15.0−1.80 (1.80−1.85)	48.8−1.90 (1.90−1.95)	49.1−1.90 (1.90−1.95)	30.0−2.28 (2.28−2.34)	138.8−2.10 (2.10−2.16)	48.34−2.30 (2.30−2.36)	20.0−2.30 (2.30−2.36)
no. of reflections ($F > 0\sigma$)	155432 (10993)	127364 (9382)	133609 (9898)	75008 (3894)	90726 (3894)	74661 (5507)	75242 (5241)
$R_{working}$ (%)	15.8 (24.4)	17.3 (28.5)	21.5 (37.3)	19.8 (32.6)	18.2 (19.6)	19.2 (27.5)	25.5 (28.7)
R_{free} (%)	18.8 (27.1)	20.4 (28.3)	26.1 (40.0)	23.1 (35.7)	21.7 (23.3)	23.6 (29.3)	30.2 (35.8)
rmsd for bond lengths (Å)	0.014	0.017	0.023	0.010	0.015	0.010	0.013
rmsd for bond angles (deg)	1.78	1.90	2.25	1.62	1.77	1.59	1.80
temperature factor (Å^2)							
polypeptide, cofactors, ligand, solvent	10.6, 9.8, 22.1, 25.7	33.2, 24.2, 23.0, 43.1	18.2, 19.7, 36.5, 24.8	23.0, 24.3, 41.9, 22.6	36.7, 29.3, 32.8, 42.1	20.4, 22.0, 60.4, 22.1	7.2, 7.8, 20.4, 10.0
PDB entry	3MM5	3MM6	3MM7	3MM8	3MM9	3MMA	3MMB

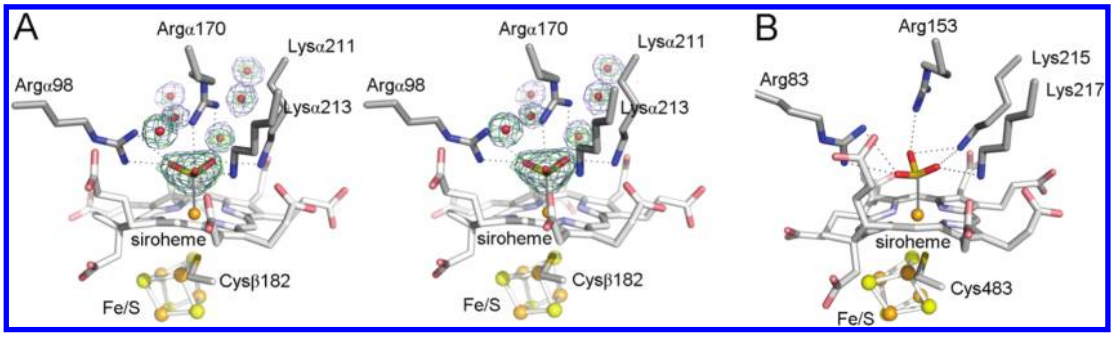

FIGURE 3: Structure of the dSir−SO_3^{2-} adduct (stereoview) (A) and the aSir−SO_3^{2-} adduct (B). In dSir and aSir, sulfite, the positively charged side chains, the siroheme carboxylates, and solvent molecules form a tight network of hydrogen bonds. The $2F_o - F_c$ (blue) and omit $F_o - F_c$ (green) electron density maps of the dSir−SO_3^{2-} structure are contoured at 1.5σ and 5.0σ, respectively. Two water molecules of the solvent network are directly hydrogen-bonded to O1 and O3 of sulfite, while O2 is shielded from bulk solvent.

Preparation of Crystalline Complexes of dSir and Reactions in Crystallo. Crystals were obtained by the hanging-drop method with the reservoir solution of 100 mM sodium citrate (pH 6.5), 20% PEG 4000, 0.2 M NaCl, and 5% (v/v) 2-propanol (*17*). The crystals were grown and prepared for data collection in a Coy anaerobe chamber (95% N_2 and 5% H_2). The space group was determined to $P2_1$, and the asymmetric unit contains one $\alpha_2\beta_2$ heterotetramer. The soaking conditions for the complexes with SO_3^{2-}, S^{2-}, NO_2^-, NO_3^-, PO_4^{3-}, CN^-, and CO are listed in Table 1. In the case of cyanide and sulfide, the crystals of dSir were reduced in the reservoir buffer supplemented with 10 mM Cr(II) EDTA (*36*); for the complexes with CO and NO, the crystals were mounted in an airtight pressure chamber and exposed to either gas for 20 min at ~1 bar. For flash-cooling in liquid nitrogen, the reservoir solution was supplemented with 15% (v/v) glycerol.

Structure Determination. Data were collected on beamlines PXI and PXII of the Swiss Light Source (SLS) at the Paul-Scherrer Institut in Villigen, Switzerland (Table 1), and processed with the HKL and XDS program suites (*37*, *38*). Statistics of data sets are summarized in Table 1. Phases were calculated from the dSir structure [Protein Data Bank (PDB) entry 3MMC] obtained from the enzyme purified and crystallized in an anaerobic tent (*17*). Refinement was performed with Refmac5 (*39*) within the CCP4 program suite (*40*). COOT (*41*) was applied for model building into the electron density. Figures were generated using PYMOL (Schrödinger, LLC). Refinement parameters and PDB entries are included in Table 1.

RESULTS AND DISCUSSION

Active Site Funnel. The substrate sulfite, or related inorganic anions like nitrite or phosphate, has to approach the active site of dSir via a 15 Å long funnel, with a size of 10 Å × 15 Å at its entrance and approximately 6 Å × 9 Å at the substrate-binding pocket located at its bottom in front of the siroheme iron (Figure 1B). The outer zone of the funnel is mainly occupied by the positively charged residues Argα80, Argα358, Hisα64, and Hisβ141. On one hand, they attract and guide the negatively charged substrate to the siroheme-[4Fe-4S] active site; on the other hand, they compensate for the negative charges of the siroheme propionate and acetate substituents. In dSir of *Desulfovibrio desulfuricans* (*18*), the funnel shape is conserved but almost completely occupied by the C-terminal arm of subunit γ, whereas in aSir (*14*, *15*), the funnel is less defined mainly because of the absence of the ferredoxin domain of subunit β.

The substrate binding pockets of dSir and aSir are mainly built up of the siroheme and side chains of Argα98, Argα170, Lysα211, and Lysα213 (*14*), termed catalytic residues (Figures 3 and 4). The carboxylate groups of the siroheme are integral components of the active site structure because they form a tight network of ion pairs together with the positively charged residues mentioned above and the substrate (Figure 1B). The thereby generated electric field is responsible for the presence of nearly 20 solvent molecules in the funnel that are firmly bound in well-defined positions [detected in the 1.8 Å structure of the dSir−sulfite complex (Figure 1B)]. aSir also harbors such a solvent cluster, albeit with a smaller number of firmly bound water molecules, and dSir from *D. desulfuricans* hosts the C-terminal end of subunit γ in the active site funnel and a few solvent molecules.

Both the active site funnel and the substrate binding pocket do not seem to undergo a major conformational change upon binding of sulfite, or the other six ligands investigated by us as documented by the low overall rmsd being between 0.2 and 0.4 Å. Most likely, the side chains of the catalytic residues cannot move significantly because of their strong fixation by their surrounding. Interestingly, the mode of fixation differs between dSir and aSir, which also results in different side chain conformations (Figure 3). In all dSir complexes investigated, the ammonium group of Lysα211 is fixed by salt bridges to the acetate carboxylate of ring C and the propionate carboxylate of ring D. Lysα211 is in van der Waals contact with Tyrα210 (Arg214 in aSir of *E. coli*) and Argα360 (Lys306 in aSir) both interacting with the propionate/acetate group of ring D. Notably, the propionate of ring D also interacts with the carbonyl oxygen of Pheα317, which forms a non-prolyl *cis* bond to Valα318. The side chain of Lysα213 is fixed by salt bridges to the ring C propionate and acetate carboxylates. Arg98 is tied via solvent molecules to Thrα96, Thrα133, Aspα135, and Thrα171, Argα170 is tightly fixed by hydrogen bonds mainly to Glyα166 and Aspα168. The corresponding Arg153 in aSir of *E. coli* is turned away.

Reduction of Sulfite, Trithionate, and Thiosulfate. (*i*) *Enzyme Activity and Product Analysis*. The specific activity for the reduction of sulfite, thiosulfate, and trithionate was measured at 83 °C over the pH range of 5−8. Maximal activity was observed at approximately pH 6.0 for all three sulfur oxide substrates (Figure 2). An activity of 56.2 ± 10.2 milliunits (pH 7) for sulfite agrees with values reported earlier for dSir from *A. fulgidus* (*42*). Thiosulfate exhibited a slightly higher activity than sulfite, whereas trithionate was less active than sulfite under our experimental conditions (Figure 2). Product analysis of trithionate, thiosulfate, and sulfide was performed by spectroscopic methods, and H_2S was additionally verified by the formation of the colored CdS and PbS. Using the

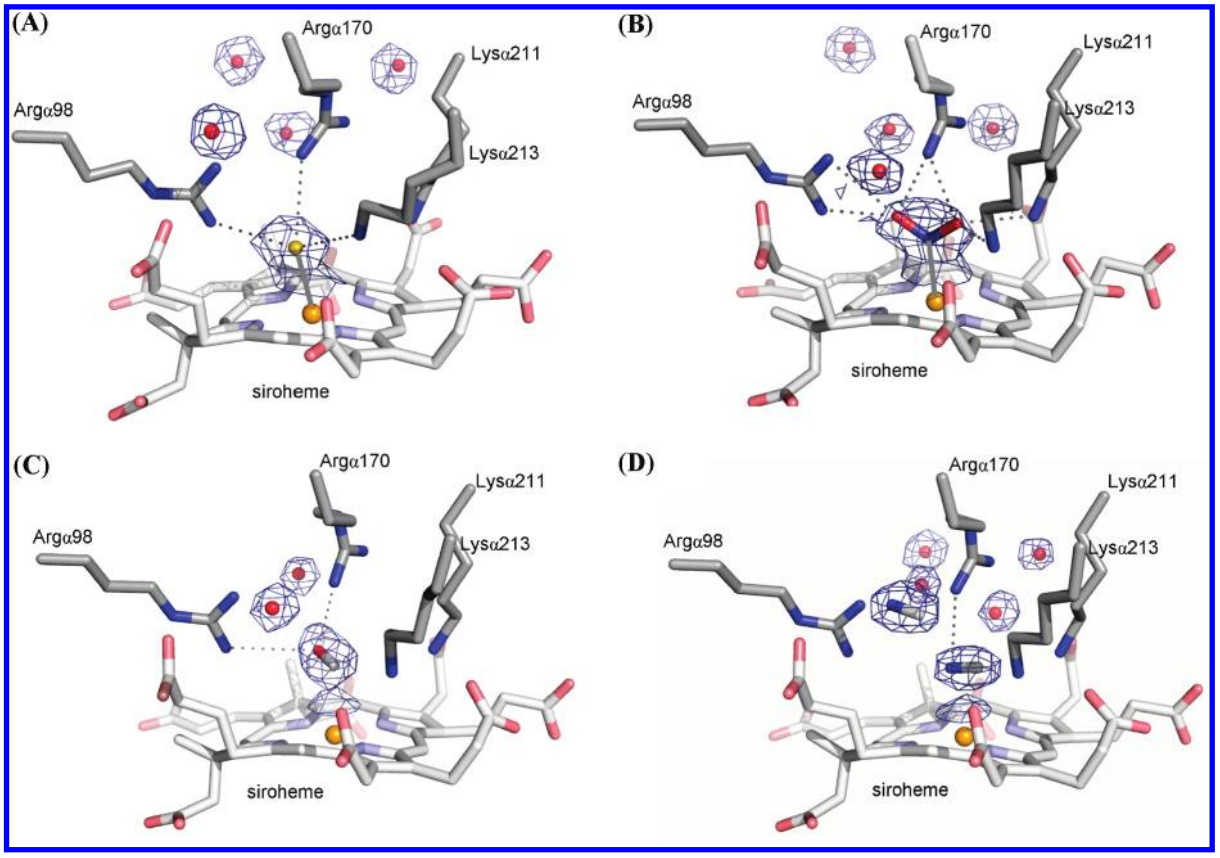

FIGURE 4: Structures of dSir in complex with S^{2-} (A), NO_2^- (B), CO (C), and CN^- (D). The electron densities are contoured at 1.5σ. The catalytic residues do not require large rearrangement over the course of catalysis, which may allow the reaction to proceed faster. The orientation of the figures is as in Figure 3.

methylviologen/deazaflavin system, sulfite reduction revealed the formation of trithionate, thiosulfate, and sulfide. Thiosulfate and sulfide were detected as products when reducing trithionate, and sulfide was detected when reducing thiosulfate.

(*ii*) *Structure of the dSir*−SO_3^{2-} *Complex*. The structure of dSir in a complex with its substrate sulfite could be established at 1.8 Å resolution (Figure 3), after crystals of the purified enzyme had been soaked with sulfite under anoxic conditions (Table 1). A dSir−SO_3^{2-} adduct could be also obtained upon soaking of dSir crystals with thiosulfate and trithionate in the reservoir solution, indicating that these sulfur oxyanions were turned over in crystallo. Attempts to crystallize the complexes of dSir of *A. fulgidus* with thiosulfate or trithionate failed as they were converted to either sulfite or sulfide depending on the experimental conditions.

The high quality of the data allowed the detection of the individual positions of the sulfite oxygens and an accurate description of the interactions of sulfite with the polypeptide backbone (Figure 3A). The sulfite molecule is present in the expected trigonal pyramidal arrangement with the sulfur tetrahedrally coordinated by the three oxygens and the siroheme iron. The iron atom sits approximately in the center of the tetrahydropyrrole ring and is bound to the sulfite sulfur (bond length of 2.3 Å) and to the thiolate sulfur of Cysβ182 (bond length of 2.6 Å) linked to the [4Fe-4S] cluster. In comparison, the siroheme iron atom of the unproductive and putative glycerol-bound active site (Figure S1 of the Supporting Information) is slightly displaced toward Cysβ182 at the proximal binding site. All three sulfur−oxygen distances of sulfite are ~1.45 Å, suggesting that dSir binds SO_3^{2-} and not HSO_3^- as found in aSir of *E. coli* (*43*). The sulfite oxygen atoms are strongly anchored to the four catalytic residues. O1 of the substrate anion is hydrogen bonded to the positively charged Lysα211 N_ζ and Argα170 $N_{\eta 2}$ atoms as well as to a solvent molecule linked to the siroheme-[4Fe-4S] cofactor (Figure 3A). O2 strongly interacts with the Lysα213 N_ζ and Argα170 $N_{\eta 1}$ atoms. The hydroxy group of Thrα133 and a solvent molecule are at distances of 4.1 and 3.7 Å, respectively, too far from O2 to form a hydrogen bond. The mentioned solvent molecule is buried inside the protein inaccessible for bulk solvent. O3 of sulfite is hydrogen bonded to the Argα98 $N_{\eta 1}$ and $N_{\eta 2}$ atoms and to a solvent molecule (Figure 3A).

The structures of the dSir−SO_3^{2-} complexes of *D. desulfuricans* (determined at 2.1 Å resolution) (*18*) and *A. fulgidus* are virtually identical, but the latter provides more accurate information about the sulfite and side chain conformations and about the solvent network. Between dSir and aSir, sulfite binding is basically conserved but also reveals unexpected differences (Figure 3). First, the sulfite ions of dSir and aSir are rotated relative to each other by approximately 60° around the iron−sulfur bond. Despite the different positions of the oxygens, their hydrogen bonding pattern has been preserved except for the exchange of Argα170 in dSir with Lys217 in aSir as the hydrogen bond partner of O2. For the optimization of the hydrogen bond geometry to the differently positioned oxygen atoms, side chain adjustments are sufficient, the largest being in the range of 1−2 Å between Argα170 and Lysα213 in dSir and Arg153 and Lys217 in aSir. Second, sulfite binding does not induce any conformational change or temperature factor increase in the structure of dSir, whereas in aSir of *E. coli*, Arg153 and some loops significantly move and the active site become more rigid. Except for sulfite, no other ligand

could trigger this conformational change in aSir of *E. coli*. In contrast to the structure of the dSir−SO_3^{2-} complex, the structure of the aSir−SO_3^{2-} complex still exhibits substantial variations between the temperature factors of siroheme, sulfite, and the polypeptide surrounding. Third, atoms O1 and O3 of sulfite are the origins for two complete but interconnected solvent chains consisting of six to eight molecules within hydrogen bonding distance of each other (Figure 1B). Therefore, the transfer of protons between the bulk solvent and sulfite via the Grotthuss mechanism (*44*) would be feasible, which would significantly accelerate their availability. Interestingly, in aSir there is space for only one solvent molecule in front of the sulfite because of conformational changes of Arg153 (Argα170 in dSir) and especially Lys215 (Lysα211 in dSir). The latter is induced by the different conformation of ring D propionate caused by a different protein environment.

(*iii*) *Structure of the dSir*−S^{2-} *Complex*. We obtained the dSir−S^{2-} complex by soaking crystals of dSir with sodium sulfide (Table 1). Its X-ray structure at 2.3 Å resolution revealed the sulfide as a spherical peak in front of the siroheme cofactor forming a covalent bond (2.7 Å) to the siroheme iron (Figure 4A). The side chains of the catalytic residues Argα98, Argα170, and Lysα213 (Lysα211 holds its position) move in the range of 0.2−0.4 Å toward the sulfur atom. Smaller distances like the observed ones (3.2−3.7 Å) are geometrically possible but presumably prevented by an increasing level of repulsion of their positively charged side chains and by their strong fixation to the siroheme carboxylates and the protein matrix (Figure 4A). A stronger sulfide binding would also cause product inhibition, which is biochemically not desirable. In comparison, the sulfur atom of the aSir−S^{2-} adduct was partially oxidized to a compound not clearly identified (*43*).

Reaction of dSir with Nitrite and Hydroxylamine

(*i*) *Enzymatic Activity*. The enzymatic activity of dSir of *A. fulgidus* was determined for the reduction of nitrite and hydroxylamine to ammonia at 83 °C at different pH values (data not shown). The specific activity of 12.5 nmol of nitrite min^{-1} mg^{-1} at pH 7 is low compared to the value of 56.2 nmol of sulfite min^{-1} mg^{-1} but is comprehensible as nitrite is not the natural substrate. In cytochrome *c* nitrite reductase, the activity of nitrite to ammonia is higher than that of sulfite to H_2S, which is still higher than that of the sulfite reduction catalyzed by dSir (*45*). In contrast to sulfite, the nitrite reductase activity of dSir increases with an increase in pH. The specific activity of 6 nmol min^{-1} mg^{-1} for hydroxylamine is rather low but demonstrates its potential role as an intermediate during the reduction of nitrite to ammonia, perhaps in a manner equivalent to that reported for cytochrome *c* nitrite reductase (*46*).

(*ii*) *Structure of the dSir*−NO_2^- *Complex*. Soaking experiments were performed with nitrite, hydroxylamine, and NO. Upon exposure to NO, the crystals of dSir immediately cracked. dSir soaked with hydroxylamine or nitrite (Table 1) resulted in a dSir−NO_2^- complex as shown by a subsequent structure analysis. Presumably, hydroxylamine decomposes prior to siroheme binding as reported for aSir (*43*).

The structure of the dSir−NO_2^- complex was determined at a resolution of 2.0 Å, which allowed the assignment of the individual atoms of nitrite (Figure 4B). Accordingly, nitrogen and not oxygen is bound to the iron of the siroheme, the distance between them being 1.95 Å. The Fe−N−O angles are 113° and 127°. In contrast to the oxygens of sulfite, the oxygens of nitrite are positioned highly similarly in dSir and aSir. Upon superimposition of the dSir−NO_2^- and dSir−SO_3^{2-} structures, O1 is located in a position equivalent to the position of O3 of sulfite (Figure 5A) and interacts with the side chains of Argα98 $N_{\eta 2}$ and Argα170 $N_{\eta 1}$. O2 of nitrite approximately sits between O1 and O2 of sulfite and is hydrogen-bonded to Argα170 $N_{\eta 1}$, Lysα211 N_ζ, and Lysα213 N_ζ. The interactions between the polypeptide and nitrite are conserved between dSir and aSir except for Argα170 (Arg153 in aSir), which adopts in aSir a different conformation.

Structures of Other dSir−*Ligand Complexes*. (*i*) *dSir*−*CO and dSir*−CN^- *Complexes*. The structures of dSir in complex with CO and CN^- were determined both at 1.9 Å resolution and characterized by the absence of a covalent contact between the siroheme and these compounds (Figure 4C,D). Their iron−carbon distances are both 2.7 Å. This finding is compatible with their nonlinear binding reflected in Fe−C−O and Fe−C−N^- angles of approximately 101° and 70°. Although the $2F_o - F_c$ electron density of the dSir−CN^- adduct is well-defined, the orientation of the CN^- can not be considered as unequivocal (resolution too low to distinguish between carbon and nitrogen) mainly because of the parallel arrangement between the siroheme ring and the bond between carbon and nitrogen. Depending on the orientation, the latter interact with Argα170 $N_{\eta 1}$ or Lysα213 N_ζ. CO is less occupied than CN^-, but the orientation appears to be clear. The oxygen atom of CO with dSir virtually corresponds to the position of O1 of nitrite (Figure 4B) and interacts with a solvent molecule, Argα98 $N_{\eta 2}$, and Argα170 $N_{\eta 1}$. The unusual CO and CN^- binding mode might be due to the proximity of Argα170, which would substantially collide with CO and CN^- in a linear arrangement (Figure 4C,D). In aSir, both the Fe−C−O and Fe−C−N angles are nearly 180° and the iron−carbon distances are 1.6 and 1.8 Å, which represent values normally found for heme−Fe−CO complexes (*43*).

(*ii*) *dSir*−NO_3^- *Complex*. The dSir−NO_3^- complex was structurally characterized at 2.3 Å resolution (Figure S2 of the Supporting Information). Hereby, nitrate is bound in a trigonal planar conformation, with both nitrogen and oxygen atoms in van der Waals contact with the siroheme ring. NO_3^- is not coordinated to the iron of the siroheme but is laterally displaced from the siroheme center such that O2 is with a distance of 2.7 Å closer to the iron than the nitrogen with a distance of 3.1 Å. The nitrate oxygens are multiply connected with the polypeptide (Figure S2 of the Supporting Information). O1 interacts with Lysα211 N_ζ (2.7 Å) and Argα170 $N_{\eta 2}$ (2.9 Å), O2 with both Argα170 $N_{\eta 1}$ (3.1 Å) and Lysα213 N_ζ (3.4 Å), and O3 with Argα98 $N_{\eta 2}$ (2.8 Å).

(*iii*) *dSir*−PO_4^{3-} *Complex*. The structure of the dSir−PO_4^{3-} complex was determined at a resolution of 2.3 Å. The tetrahedral PO_4^{3-} anion is coordinated via O4 to the iron of the siroheme (Figure S3 of the Supporting Information). The Fe−O4 distance is 1.6 Å, which is the shortest between iron and the ligands characterized in this study. O1 of phosphate interacts with Lysα211 N_ζ (2.3 Å) and Argα170 $N_{\eta 2}$ (3.3 Å), O2 with Lysα213 N_ζ (3.2 Å) and Argα170 $N_{\eta 1}$ (2.5 Å), and O3 with Argα98 $N_{\eta 2}$ (3.2 Å), Argα170 $N_{\eta 1}$ (3.2 Å), and Argα170 $N_{\eta 2}$ (3.4 Å). An interesting aspect of the structure of the dSir−NO_3^- and dSir−PO_4^{3-} complexes is that their O1, O2, and O3 atoms are at virtually identical positions compared to those of sulfite in the dSir−sulfite complex (Figure 5A).

Reaction of dSir. The proposed catalytic mechanism for dSir outlined in Figure 5B is based on several properties of the active site, on the electron supply mode that is thought to consist of three consecutive two-electron transfer processes, and, most

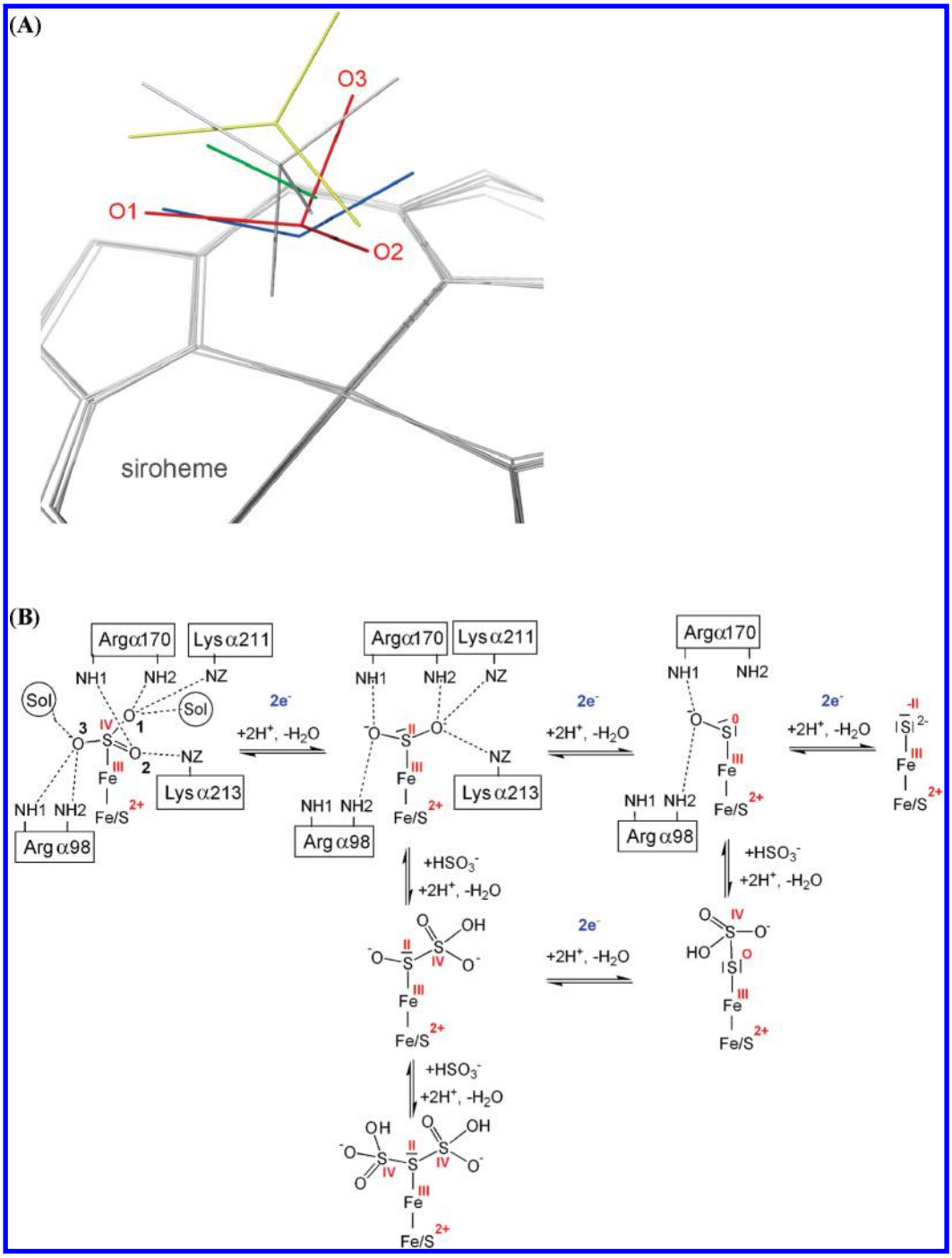

FIGURE 5: Reaction of dSir from *A. fulgidus*. (A) Superposition of the dSir−SO_3^{2-} (red), −NO_2^- (blue), −CO (green), −NO_3^- (yellow), and −PO_4^{3-} (gray) structures. The dSir−NO_2^- and dSir−CO structures might resemble those of the short-lived dSir−SO_2^{2-} and dSir−SO^- intermediates. The positions of the oxygen atoms of the sulfur−oxygen compounds suggest the order of their dehydration. (B) Scheme of the six-electron reduction cycle of sulfite to sulfide. Only residues that directly interact with the siroheme iron-bound sulfur−oxygen adduct are colored. The process is subdivided into three two-electron transfer steps each accompanied by acceptance of two protons and release of one H_2O molecule. Trithionate and thiosulfate might be produced if the S(II) and S(0) intermediates are sufficiently long-living to be attacked by a sulfite; these side reactions are supported by high sulfite concentrations that are unlikely to exist within the cell.

importantly, on the experimentally determined structures of the dSir−ligand complexes (Figure 5A). A related reduction−dehydration scenario for the transformation of sulfite to H_2S was reported earlier for aSir (*43*) and could also be formulated for the reduction of nitrite to ammonia.

First, the basic features of sulfite reduction are well conserved in aSir and dSir because of the related size, shape, and electrostatics of the active site pocket and the common siroheme-based substrate binding. The strictly conserved catalytic residues Argα98, Argα170, Lysα211, and Lysα213 characterized by their positive charge and torsional flexibility of their long side chains are perfectly suited to bind and polarize negatively charged sulfur−oxygen species with varied shape and charge (Figures 3 and 4) and to facilitate thereby the release of OH^- or H_2O. The generated electric field creates a network of firmly bound solvent molecules that presumably serve as a proton source for dehydration. The measured maximal specific activity at pH 6 suggests that the availability of protons accelerates the reaction.

Second, the electron supply mode is derived from a property of the coupled siroheme-Fe/S cofactor to accept merely two electrons at once (*47*) and from the found in vitro formation of trithionate and thiosulfate implying Fe−sulfur−oxygen intermediates in oxidation states +II and 0, with a sufficiently long lifetime to allow a nucleophilic attack of sulfite. Thus, each of the three consecutive steps might consist of a reduction and a dehydration reaction between sulfur compounds with three oxygens, two oxygens, or one oxygen in oxidation states IV, II, and 0, respectively (Figure 5B).

Third, dSir bound to its substrate sulfite and its product sulfide has been structurally characterized (Figures 3 and 4), whereas the structures of the postulated reaction intermediates (dSir−Fe−SO_2^- and dSir−Fe−SO^-) are assumed to resemble those of the experimentally accessible dSir−NO_2^- and dSir−CO complexes (Figure 4B,C). As a consequence of the sequential dehydration mechanism (Figure 5B), it is assumed that O3 of sulfite in the position not present in NO_2^- and CO is abstracted at first and O1 shared by SO_3^{2-}, NO_2^-, and CO at last (Figure 5A). Moreover, the solvent hydrogen-bonded to O3 interacts with the ring D acetate carboxylate group, thus improving the proton acceptor properties of O3 compared to those of O1 and O2.

Accordingly, O3 of sulfite is protonated at first by the adjacent water molecule of the solvent network (or is already protonated when bound as bisulfite) and released as OH^-, which is concomitantly protonated to H_2O. If the structure of the dSir−Fe−NO_2^- complex (with a planar nitrite bound to iron) represents a reasonable model for the dSir−Fe−SO_2^- intermediate, O2 of sulfite is placed between the positions of O2 and O3 of sulfite (Figure 5A). Subsequently, the S−O2 bond becomes activated by a two-electron transfer and released as OH^- after protonation via an adjacent water molecule of the solvent network. Finally, O1 of the dSir−Fe−SO^- intermediate positioned as in the Fe−CO structure is released after two-electron reduction and subsequent protonation, thereby generating the experimentally observed Fe−S^{2-} adduct (Figure 4A). A new aspect was added to the discussion of the sulfite reduction mechanism by the structure of the *D. vulgaris* dSir (*18*), which suggested a cysteine thiol group of subunit γ of dSir acts as an electron donor for the terminal two-electron reduction.

Despite their pronounced active site relationship described above, the catalytic capability of dSir and aSir differs at least under in vitro conditions (*48*) with respect to their substrate specificity and product profile. While aSir solely uses sulfite as a sulfur-containing substrate that is converted to sulfide without detectable reaction intermediates (*49*, *50*), dSir, in addition, can both convert and produce trithionate and thiosulfate. These findings also hold true for dSir of *A. fulgidus*, which was the first archaeal sulfate-reducing microorganism studied in vitro with respect to its substrate and product specificity. This difference between dSir and aSir can be structurally rationalized. In dSir, the Fe−sulfur−oxygen intermediates are accessible for sulfite from the active site channel (Figures 1 and 3), allowing a nucleophilic attack if the six-electron delivery does not proceed sufficiently rapidly. Thus, thiosulfate can be directly produced from an Fe−S(0) oxygen intermediate (Figure 5B), whereas the formation of trithionate requires conformational changes of the polypeptide chain if two sulfite molecules have to be bound simultaneously in front of the Fe−S(II) oxygen intermediate. In contrast, a van der Waals contact between an incoming sulfite ion and a sulfur−oxygen atom is prevented in aSir because of the conformational change in Arg153 and, in particular, Lys215. The displacement of the latter residue is induced by a substantial rearrangement of the ring D propionate in aSir compared to dSir because of their different protein surroundings.

The process of in vivo sulfite reduction by sulfate-reducing microorganisms has been a matter of controversy for more than 40 years. It resulted in two alternative reaction mechanisms, although the application of both cannot be ruled out depending on the organism and environmental conditions. In the first mechanism, sulfite is reduced to sulfide without the liberation of intermediates. The formation of thiosulfate and trithionate accounts consequently for the incompetence of the in vitro reduction system to drive the complete six-electron transfer reaction. Most likely, the multielectron transfer step must be much more complex than in aSir because of its integration into the energy conservation machinery. This view is corroborated by a large number of data documenting that the formation of trithionate, thiosulfate, and sulfide and their relative ratios highly depend on a number of experimental conditions, such as pH, the nature of the electron donor and its concentration, and the sulfite concentration (*51*). The second mechanism termed the trithionate pathway comprises the reduction of sulfite to sulfide via the enzymes sulfite reductase, thiosulfate reductase, and trithionate reductase with trithionate and thiosulfate as free intermediates (*48*). Indicative of the trithionate pathway appears to be the predominant formation of trithionate by dSir and, in parallel, its inability to efficiently metabolize trithionate and thiosulfate. The trithionate pathway gains some support with the finding that in some organisms a trithionate reductase and/or a thiosulfate reductase have been partially characterized (*52*−*54*). However, their physiological role has not been definitively worked out and has been questioned by a recent genetic experiment (*55*) demonstrating that impaired thiosulfate reduction does not affect the ability of the organism to grow on sulfate and H_2. As measured, purified *A. fulgidus* dSir is able to reduce in vitro besides sulfite trithionate and thiosulfate to H_2S (Figure 2). No further enzymes are required, although genes encoding trithionate and thiosulfate reductase-related enzymes are present in the genome of *A. fulgidus* (*56*). Their functions in the cell are, however, not established. We included the trithionate and thiosulfate metabolism in Figure 5B according to a scheme reported 35 years ago (*57*, *58*), which does, however, not argue against a one-step sulfite reduction mechanism for dSir of *A. fulgidus* in vivo. For unravelling the mechanism of dissimilatory sulfite reduction, detailed information about the energy conservation system of sulfate-reducing organisms is required, in particular, about the molecular components of their electron transfer pathway. Energetic considerations demand an electron transport-linked phosphorylation process (*3*), and experimental data clearly demonstrated that the reductive process is influenced by membrane-associated steps (*32*, *59*).

ACKNOWLEDGMENT

We thank Harald Huber (University of Regensburg, Regensburg, Germany) for the generous supply of *A. fulgidus* cells, Hartmut Michel (MPI of Biophysics, Frankfurt, Germany) for continuous support, and the staff of beamlines PXI and PXII at the Swiss Light Source for help during data collection.

SUPPORTING INFORMATION AVAILABLE

Structures of dSir in complex with glycerol, nitrate, and phosphate (Figures S1−S3, respectively). This material is available free of charge via the Internet at http://pubs.acs.org.

REFERENCES

1. Canfield, D. E., Rosing, M. T., and Bjerrum, C. (2006) Early anaerobic metabolisms. *Philos. Trans. R. Soc. London, Ser. B 361*, 1819–1835.
2. Hansen, T. A. (1994) Metabolism of sulfate-reducing prokaryotes. *Antonie van Leeuwenhoek 66*, 165–185.
3. Thauer, R. K., Stackebrandt, E., and Hamilton, W. A. (2007) Energy metabolism and phylogenetic diversity of sulphate-reducing bacteria. In Sulphate-reducing bacteria: Environmental and engineered systems (Barton, L. L., and Hamilton, W. A., Eds.) pp 1−37, Cambridge University Press, Cambridge, U.K.
4. Schwenn, J. D. (1997) Assimilatory reduction of inorganic sulfate. In Sulfur nutrition and assimilation in higher plants (Cram, J. W., Ed.) pp 3−23, Academic Publishing, The Hague, The Netherlands.
5. Crane, B. R., and Getzoff, E. D. (1996) The relationship between structure and function for the sulfite reductases. *Curr. Opin. Struct. Biol. 6*, 744–756.
6. Stroupe, M. E., and Getzoff, E. D. (2001) Sulfite reductase hemoprotein. In Handbook of Metalloproteins (Messerschmidt, A., Huber, R., Poulus, T., and Wieghardt, K., Eds.) pp 471−485, John Wiley & Sons, Chichester, U.K.
7. Dhillon, A., Goswani, S., Riley, M., Teske, A., and Sogin, M. (2005) Domain evolution and functional diversification of sulfite reductases. *Astrobiology 5*, 18–29.
8. Moura, I., LeGall, J., Lino, A. R., Peck, H. D., Fauque, G., Xavier, A. V., DerVartanian, D. V., Moura, J. J. G., and Huynh, B. H. (1988) Characterization of two dissimilatory sulfite reductases (desulforubinin and desulfoviridin) from sulfate-reducing bacteria. Mössbauer and EPR studies. *J. Am. Chem. Soc. 110*, 1075–1082.
9. Price-Carter, M., Tingey, J., Bobik, T. A., and Roth, J. R. (2001) The alternative electron acceptor tetrathionate supports B12-dependent anaerobic growth of *Salmonella enterica* serovar *typhimurium* on ethanolamine or 1,2-propanediol. *J. Bacteriol. 183*, 2463–2475.
10. Wagner, M., Roger, A. J., Flax, J. L., Brusseau, G. A., and Stahl, D. A. (1998) Phylogeny of dissimilatory sulfite reductases supports an early origin of sulfate respiration. *J. Bacteriol. 180*, 2975–2982.
11. Murphy, M. J., and Siegel, L. M. (1973) Siroheme and sirohydrochlorin. The basis for a new type of porphyrin-related prosthetic group common to both assimilatory and dissimilatory sulfite reductases. *J. Biol. Chem. 248*, 6911–6919.
12. Siegel, L. M., Rueger, D. C., Barber, M. J., Krueger, R. J., Orme-Johnson, N. R., and Orme-Johnson, W. H. (1982) *Escherichia coli* sulfite reductase hemoprotein subunit. Prosthetic groups, catalytic parameters, and ligand complexes. *J. Biol. Chem. 257*, 6343–6350.
13. Marritt, S. J., and Hagen, W. F. (1996) Dissimilatory sulfite reductase revisited. The desulfoviridin molecule does contain 20 iron ions, extensively demetallated sirohaem, and an S = 9/2 iron-sulfur cluster. *Eur. J. Biochem. 238*, 724–727.
14. Crane, B. R., Siegel, L. M., and Getzoff, E. D. (1995) Sulfite reductase structure at 1.6 Å: Evolution and catalysis for reduction of inorganic anions. *Science 270*, 59–67.
15. Schnell, R., Sandalova, T., Hellman, U., Lindqvist, Y., and Schneider, G. (2005) Siroheme- and [Fe4-S4]-dependent NirA from *Mycobacterium tuberculosis* is a sulfite reductase with a covalent Cys-Tyr bond in the active site. *J. Biol. Chem. 280*, 27319–27328.
16. Swamy, U., Wang, M., Tripathy, J. N., Kim, S. K., Hirasawa, M., Knaff, D. B., and Allen, J. P. (2005) Structure of spinach nitrite reductase: Implications for multi-electron reactions by the iron-sulfur: siroheme cofactor. *Biochemistry 44*, 16054–16063.
17. Schiffer, A., Parey, K., Warkentin, E., Diederichs, K., Huber, H., Stetter, K. O., Kroneck, P. M., and Ermler, U. (2008) Structure of the dissimilatory sulfite reductase from the hyperthermophilic archaeon *Archaeoglobus fulgidus*. *J. Mol. Biol. 379*, 1063–1074.
18. Oliveira, T. F., Vonrhein, C., Matias, P. M., Venceslau, S. S., Pereira, I. A., and Archer, M. (2008) The crystal structure of *Desulfovibrio vulgaris* dissimilatory sulfite reductase bound to DsrC provides novel insights into the mechanism of sulfate respiration. *J. Biol. Chem. 283*, 34141–34149.
19. Steuber, J., Arendsen, A. F., Hagen, W. R., and Kroneck, P. M. (1995) Molecular properties of the dissimilatory sulfite reductase from *Desulfovibrio desulfuricans* (Essex) and comparison with the enzyme from *Desulfovibrio vulgaris* (Hildenborough). *Eur. J. Biochem. 233*, 873–879.
20. Pierik, A. J., Wolbert, R. B., Mutsaers, P. H., Hagen, W. R., and Veeger, C. (1992) Purification and biochemical characterization of a putative [6Fe-6S] prismane-cluster-containing protein from *Desulfovibrio vulgaris* (Hildenborough). *Eur. J. Biochem. 206*, 697–704.
21. Mizuno, N., Voordouw, G., Miki, K., Sarai, A., and Higuchi, Y. (2003) Crystal structure of dissimilatory sulfite reductase D (DsrD) protein: Possible interaction with B- and Z-DNA by its winged-helix motif. *Structure 11*, 1133–1140.
22. Mander, G. J., Weiss, M. S., Hedderich, R., Kahnt, J., Ermler, U., and Warkentin, E. (2005) X-ray structure of the γ-subunit of a dissimilatory sulfite reductase: Fixed and flexible C-terminal arms. *FEBS Lett. 579*, 4600–4604.
23. Cort, J. R., Mariappan, S. V., Kim, C. Y., Park, M. S., Peat, T. S., Waldo, G. S., Terwilliger, T. C., and Kennedy, M. A. (2001) Solution structure of *Pyrobaculum aerophilum* DsrC, an archaeal homologue of the γ subunit of dissimilatory sulfite reductase. *Eur. J. Biochem. 268*, 5842–5850.
24. Knaff, D. B. (1996) Ferredoxin and ferredoxin-dependent enzymes. In Oxygenic photosynthesis: The light reactions (Ort, D. R., and Yocum, C. F., Eds.) pp 333−361, Kluwer Publishers, Dordrecht, The Netherlands.
25. Siegel, L. M., Murphy, M. J., and Kamin, H. (1973) Reduced nicotinamide adenine dinucleotide phosphate-sulfite reductase of enterobacteria. I. The *Escherichia coli* hemoflavoprotein: Molecular parameters and prosthetic groups. *J. Biol. Chem. 248*, 251–264.
26. Hatchikian, E. C., and Zeikus, J. G. (1983) Characterization of a new type of dissimilatory sulfite reductase present in *Thermodesulfobacterium commune*. *J. Bacteriol. 153*, 1211–1220.
27. Stetter, K. O., Lauerer, G., Thomm, M., and Neuner, A. (1987) Isolation of Extremely Thermophilic Sulfate Reducers: Evidence for a Novel Branch of Archaebacteria. *Science 236*, 822–824.
28. Smith, P. K., Krohn, R. I., Hermanson, G. T., Mallia, A. K., Gartner, F. H., Provenzano, M. D., Fujimoto, E. K., Goeke, N. M., Olson, B. J., and Klenk, D. C. (1985) Measurement of protein using bicinchoninic acid. *Anal. Biochem. 150*, 76–85.
29. Büchert, T. (2001) Structure and function of adenosine 5′-phosphosulfate reductase. Dissertation, Universität Konstanz, Konstanz, Germany.
30. Boltz, D. F., and Taras, M. J. (1978) Nitrogen. In Colorimetric determination of nonmetals. Chemical analysis (Boltz, D. F., and Howell, J. A., Eds.) pp 197−251, John Wiley & Sons Inc., New York.
31. Kelly, D. P., Chambers, L. A., and Trudinger, P. A. (1969) Cyanolysis and spectrophotometric estimation of trithionate in mixture with thiosulfate and tetrathionate. *Anal. Chem. 41*, 898–901.
32. Fitz, R. M., and Cypionka, H. (1990) Formation of thiosulfate and trithionate during sulfite reduction by washed cells of *Desulfovibrio desulfuricans*. *Arch. Microbiol. 154*, 400–406.
33. Fogo, J. K., and Popowsky, M. (1949) Spectrophotometric determination of hydrogen sulfide. *Anal. Chem. 21*, 732–734.
34. Cline, J. D. (1969) Spectrophotometric determination of hydrogen sulfide in natural waters. *Limnol. Oceanogr. 14*, 454–458.
35. Steuber, J. (1996) Molecular and kinetic properties of desulfoviridin, the dissimilatory ferrocytochrome c_3: sulfite oxidoreductase from *Desulfovibrio desulfuricans* (Essex). Dissertation, Universität Konstanz, Konstanz, Germany.
36. Madden, J. F., Han, S. H., Siegel, L. M., and Spiro, T. G. (1989) Resonance Raman studies of *Escherichia coli* sulfite reductase hemoprotein. 2. Fe_4S_4 cluster vibrational modes. *Biochemistry 28*, 5471–5477.
37. Otwinowski, Z., and Minor, W. (1997) Processing of X-ray diffraction data collected in oscillation mode. *Methods Enzymol. 276*, 307–326.
38. Kabsch, W. (1993) Automatic processing of rotation diffraction data from crystals of initially unknown symmetry and cell constants. *J. Appl. Crystallogr. 26*, 795–800.
39. Murshudov, G. N., Vagin, A. A., and Dodson, E. J. (1997) Refinement of macromolecular structures by the maximum-likelihood method. *Acta Crystallogr. D53*, 240–255.
40. Potterton, E., McNicholas, S., Krissinel, E., Cowtan, K., and Noble, M. (2002) The CCP4 molecular-graphics project. *Acta Crystallogr. D58*, 1955–1957.
41. Emsley, P., and Cowtan, K. (2004) Coot: Model-building tools for molecular graphics. *Acta Crystallogr. D60*, 2126–2132.
42. Dahl, C., Kredich, N. M., Deutzmann, R., and Truper, H. G. (1993) Dissimilatory sulphite reductase from *Archaeoglobus fulgidus*: Physico-chemical properties of the enzyme and cloning, sequencing and analysis of the reductase genes. *J. Gen. Microbiol. 139*, 1817–1828.
43. Crane, B. R., Siegel, L. M., and Getzoff, E. D. (1997) Probing the catalytic mechanism of sulfite reductase by X-ray crystallography: Structures of the *Escherichia coli* hemoprotein in complex with substrates, inhibitors, intermediates, and products. *Biochemistry 36*, 12120–12137.
44. de Grotthuss, C. J. T. (1806) Sur la décomposition de l′eau et des corps qu'elle tient en dissolution à l′aide de l′électricité galvanique. *Ann. Chim. 58*, 54–73.

45. Lukat, P., Rudolf, M., Stach, P., Messerschmidt, A., Kroneck, P. M., Simon, J., and Einsle, O. (2008) Binding and reduction of sulfite by cytochrome c nitrite reductase. *Biochemistry 47*, 2080–2086.
46. Einsle, O., Messerschmidt, A., Huber, R., Kroneck, P. M., and Neese, F. (2002) Mechanism of the six-electron reduction of nitrite to ammonia by cytochrome c nitrite reductase. *J. Am. Chem. Soc. 124*, 11737–11745.
47. Lui, S. M., Soriano, A., and Cowan, J. A. (1993) Enzymatic reduction of inorganic anions. Pre-steady-state kinetic analysis of the dissimilatory sulfite reductase (desulfoviridin) from *Desulfovibrio vulgaris* (Hildenborough). Mechanistic implications. *J. Am. Chem. Soc. 115*, 10483–10486.
48. Kobayashi, K., Tachibana, S., and Ishimoto, M. (1969) Intermediary formation of trithionate in sulfite reduction by a sulfate-reducing bacterium. *J. Biochem. 65*, 155–157.
49. Siegel, L. M., Davis, P. S., and Kamin, H. (1974) Reduced nicotinamide adenine dinucleotide phosphate-sulfite reductase of enterobacteria. 3. The *Escherichia coli* hemoflavoprotein: Catalytic parameters and the sequence of electron flow. *J. Biol. Chem. 249*, 1572–1586.
50. Asada, K., Tamura, G., and Bandurski, R. S. (1969) Methyl viologen-linked sulfite reductase from spinach leaves. *J. Biol. Chem. 244*, 4904–4915.
51. Agaki, J. M. (1995) Respiratory sulfate reduction. In Sulfate-reducing bacteria (Barton, L. L., Ed.) pp 89−111, Plenum Press, New York.
52. Nakatsukasa, W., and Akagi, J. M. (1969) Thiosulfate reductase isolated from *Desulfotomaculum nigrificans*. *J. Bacteriol. 98*, 429–433.
53. Kim, J. H., and Akagi, J. M. (1985) Characterization of a trithionate reductase system from *Desulfovibrio vulgaris*. *J. Bacteriol. 163*, 472–475.
54. Aketagawa, J., Kobayashi, K., and Ishimoto, M. (1985) Purification and properties of thiosulfate reductase from *Desulfovibrio vulgaris*, Miyazaki F. *J. Biochem. 97*, 1025–1032.
55. Broco, M., Rousset, M., Oliveira, S., and Rodrigues-Pousada, C. (2005) Deletion of flavoredoxin gene in *Desulfovibrio gigas* reveals its participation in thiosulfate reduction. *FEBS Lett. 579*, 4803–4807.
56. Klenk, H. P., Clayton, R. A., Tomb, J. F., White, O., Nelson, K. E., Ketchum, K. A., Dodson, R. J., Gwinn, M., Hickey, E. K., Peterson, J. D., Richardson, D. L., Kerlavage, A. R., Graham, D. E., Kyrpides, N. C., Fleischmann, R. D., Quackenbush, J., Lee, N. H., Sutton, G. G., Gill, S., Kirkness, E. F., Dougherty, B. A., McKenney, K., Adams, M. D., Loftus, B., Peterson, S., Reich, C. I., McNeil, L. K., Badger, J. H., Glodek, A., Zhou, L., Overbeek, R., Gocayne, J. D., Weidman, J. F., McDonald, L., Utterback, T., Cotton, M. D., Spriggs, T., Artiach, P., Kaine, B. P., Sykes, S. M., Sadow, P. W., D'Andrea, K. P., Bowman, C., Fujii, C., Garland, S. A., Mason, T. M., Olsen, G. J., Fraser, C. M., Smith, H. O., Woese, C. R., and Venter, J. C. (1997) The complete genome sequence of the hyperthermophilic, sulphate-reducing archaeon *Archaeoglobus fulgidus*. *Nature 390*, 364–370.
57. Drake, H. L., and Akagi, J. M. (1977) Bisulfite reductase of *Desulfovibrio vulgaris*: Explanation for product formation. *J. Bacteriol. 132*, 139–143.
58. Kobayashi, K., Seki, Y., and Ishimoto, M. (1974) Biochemical studies on sulfate-ruducing bacteria. 8. Sulfite reductase from *Desulfovibrio vulgaris*: Mechanism of trithionate, thiosulfate, and sulfide formation and enzymatic properties. *J. Biochem. 75*, 519–529.
59. Drake, H. L., and Akagi, J. M. (1978) Dissimilatory reduction of bisulfite by *Desulfovibrio vulgaris*. *J. Bacteriol. 136*, 916–923.